Check for updates

Effect of rGO–Fe$_2$O$_3$ nanocomposites fabricated in different solvents on the thermal decomposition properties of ammonium perchlorate

Ming Zhang, [iD] Fengqi Zhao,* Yanjing Yang, [iD] Jiankan Zhang, Na Li and Hongxu Gao

rGO–Fe$_2$O$_3$ composites were prepared using different solvents (distilled water, ethanol, *N*-methylpyrrolidone, ethyl acetate, *n*-butyl alcohol and *N*,*N*-dimethylformamide) *via* a simple solvothermal method and characterized by SEM, TEM, XRD, FT-IR, Raman and XPS techniques. Then, the catalytic action of rGO–Fe$_2$O$_3$ composites (prepared in different solvents), GO, rGO and pristine Fe$_2$O$_3$ on the thermal decomposition of ammonium perchlorate (AP) were studied using a TG-DSC instrument. DSC results showed that GO, rGO, pristine Fe$_2$O$_3$ and rGO–Fe$_2$O$_3$ composites could effectively promote the thermal decomposition of AP. Additionally, rGO–Fe$_2$O$_3$ fabricated in *N*,*N*-dimethylformamide (DMF) solvent possesses the best catalytic performance among the investigated materials. This result can be attributed to the better dispersibility of Fe$_2$O$_3$ nanoparticles on graphene oxide prepared in DMF solvent, which was confirmed by SEM and TEM imaging. The high temperature decomposition exothermic peak (HTP) and the apparent activation energy of AP are reduced by 119.6 °C and 173.3 kJ mol^{-1}, respectively, in the presence of Fe$_2$O$_3$–rGO (DMF) composite.

1. Introduction

Solid rocket propellant is the power source for rockets and missile engines, and its performance directly affects the operational effectiveness and survivability of missile systems. Solid propellants are usually composed of oxidants, adhesives, fuels, burning rate catalysts and other components. Oxidants are the main energy components of the propellants, and their thermal decomposition characteristics significantly affect the combustion properties of solid propellants.[1–3] Ammonium perchlorate (AP) is a commonly used oxidizer of solid rocket propellant owing to its high oxygen content, favorable physical and chemical stability.[4–7]

Nanometer-scale transition metal oxides used as burning rate catalysts could effectively promote the thermal decomposition of the oxidant and improve the combustion properties of solid propellants.[8–10] Numerous transition metal oxides, such as CuO, NiO, MnO$_2$, TiO$_2$ and Fe$_2$O$_3$ have been used as burning rate catalysts of solid propellants.[11–15] Among them, Fe$_2$O$_3$ is widely used for the promotion of thermal decomposition owing to its abundance, low cost and non-toxic properties.[16–18] Ma *et al.*[18] studied the thermal decomposition properties of AP with and without Fe$_2$O$_3$ nanoparticles. The obtained Fe$_2$O$_3$–AP

composite presented better thermal decomposition and combustion properties compared with those of pristine AP.

However, the large surface area of this nanoscale catalyst makes it easy to agglomerate, and the catalytic activity after agglomeration significantly reduced. Graphene and its derivatives have been used in the fields of catalyst loading and energetic materials owing to their large specific surface area, excellent mechanical properties, good electrical and thermal conductivity performance.[19–24] Dey *et al.*[23] fabricated rGO–Fe$_2$O$_3$ composite *via* microwave irradiation and ultrasonic treatment methods, and used it to catalyze the thermal decomposition of AP. The results indicated that the introduction of graphene could effectively promote the thermal decomposition of AP by improving the dispersion of Fe$_2$O$_3$ nanoparticles. As a commonly used method for nanomaterials fabrication, solvothermal method (water as the reaction medium) was also used for rGO–Fe$_2$O$_3$ composite fabrication. HTP of AP significantly reduced from 432 to 367 °C after mixing with the rGO–Fe$_2$O$_3$ composite.[24] It is well-known that the solvent in the solvothermal method has a great influence on the structure and properties of the as-synthesized materials. Additionally, the structure and properties of the catalytic materials directly affect the thermal decomposition properties of the catalyzed energetic materials.[25,26] However, the effect of reaction solvents on properties of rGO–Fe$_2$O$_3$ composites and the effect of fabricated rGO–Fe$_2$O$_3$ composites on the thermal decomposition properties of AP are seldom reported.

Science and Technology on Combustion and Explosion Laboratory, Xi'an Modern Chemistry Research Institute, Xi'an 710065, China.
E-mail: zhangm3210@163.com, zhaofqi@163.com

Based on this discussion, the effects of different solvents on the properties of graphene loaded ferric oxide (rGO–Fe_2O_3) nanocomposites, prepared *via* a simple one-pot solvothermal method, were studied using SEM, TEM, XRD, FT-IR, Raman and XPS techniques. In addition, the effects of the as-synthesized rGO, pristine Fe_2O_3 and rGO–Fe_2O_3 composites on AP decomposition were investigated. The apparent activation energy of AP was calculated using the Kissinger and Ozawa's methods with the obtained DSC results. Based on the abovementioned research strategy, the best rGO–Fe_2O_3 sample for thermal decomposition promotion of AP was determined, and the possible catalytic mechanisms on the thermal decomposition of AP was also analyzed (see Fig. 1).

2. Experiment

2.1 Materials

All the chemicals were of analytical grade and used without further purification. Graphite oxide (GO, C/O = 1) was purchased from Ashine Advanced Carbon Materials Co., Ltd., Changzhou. Distilled water, ethanol (EA, Xi'an Chemical Reagent Factory), *N,N*-dimethylformamide (DMF, Chron chemical Co., Ltd. of ChengDu), *N*-methylpyrrolidone (NMP, Xilong Scientific Co., Ltd. of SiChuan), ethylene glycol (EG) (EG, Sinopharm Chemical Reagent Co., Ltd.) and *n*-butyl alcohol (NBA, Chron chemical Co., Ltd. of ChengDu) were used as solvents, separately. Ammonia (Xilong Scientific Co., Ltd. of SiChuan, 25–28%) was used to adjust the pH value of solvents. Ferric nitrate hydrate ($Fe(NO_3)_3·9H_2O$) was purchased from Aladdin Inc. Ammonium perchlorate was obtained from Xi'an Modern Chemistry Research Institute.

2.2 Preparation of rGO, Fe_2O_3 and Fe_2O_3–rGO composites

Graphite oxide (60 mg) was ultrasonically dispersed in 50 mL of different solvents (six types) for 30 minutes, separately. Then, 0.2 g $Fe(NO_3)_3·9H_2O$ (dissolved in 10 mL different solvents) was added into the above six dispersions under mechanical agitation. After mixing, the pH value of the solution was adjusted to 9–10 by adding ammonia. The reactants were transformed into 100 mL Teflon-sealed autoclave and heated at 180 °C for 24 hours. After cooling, the products were washed several times with distilled water and absolute alcohol. Then, the products were cured at 60 °C in a vacuum oven overnight and ground for further characterization. Fe_2O_3 and rGO were also fabricated using the same procedure except without the addition of $Fe(NO_3)_3·9H_2O$ or GO.

2.3 Characterization

The morphology and size of GO, rGO, pristine Fe_2O_3 and rGO–Fe_2O_3 composites (prepared in different solvents) were characterized by scanning electron microscopy (SEM, Quanta600) and transmission electron microscopy (TEM, Tecnai G2 F20). Structure and composition were analyzed using X-ray diffraction (XRD, EMPYREAN), Fourier transform infrared spectroscopy (FT-IR, Bruker Tensor 27), Raman spectroscopy (RM2000, 532 nm) and X-ray photoelectron spectroscopy (XPS, Thermo scientific). XRD patterns were collected using a Cu Kα source in the measurement angle range of $2\theta = 5$–90° with a scan rate of 8° min^{-1}. The catalytic action of the rGO–Fe_2O_3 composites (prepared in different solvents), GO, rGO and pristine Fe_2O_3 on the thermal decomposition of AP (the mass ratio of AP to additive is 5) were studied by TG-DSC (NETZSCH STA449F3) with a heating rate
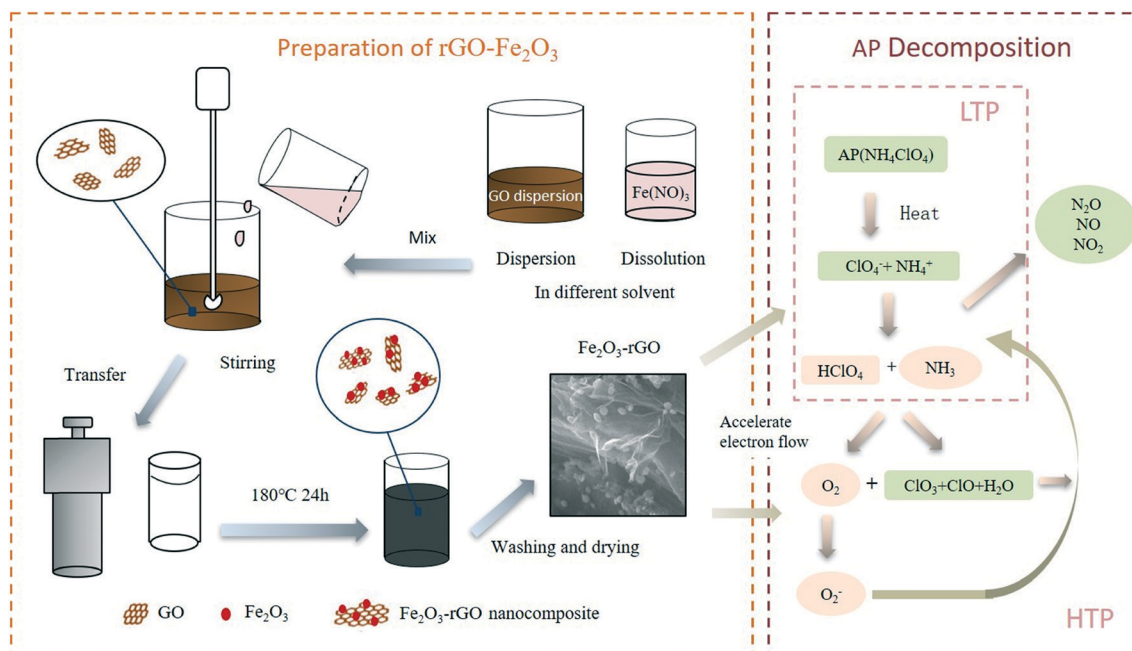

Fig. 1 Illustration of rGO–Fe_2O_3 fabrication and its catalytic mechanism for the thermal decomposition of AP.

of 5, 10, 15 and 20 °C min^{-1}. Kissinger and Ozawa's methods were employed to obtain the kinetic parameters of AP before and after mixing with different additives.

3. Results and discussion

3.1 XRD analysis

XRD patterns of GO, as-prepared rGO, pristine Fe_2O_3 and rGO–Fe_2O_3 composites (prepared in different solvents) are presented in Fig. 2. The diffraction peaks of pristine Fe_2O_3 appear at 24.2°, 33.2°, 35.6°, 40.9°, 49.5°, 54.1°, 62.4° and 64.0°, which correspond well with the crystal planes of (012), (104), (110), (113), (024), (116), (214) and (300) of hematite, respectively (JCPDS No. 33-0664).[30] In addition, the characteristic diffraction peaks of Fe_2O_3 appear in the XRD patterns of rGO–Fe_2O_3 composites (fabricated in NBA, H_2O, NMP, EA and DMF solvents), demonstrating the successful formation of Fe_2O_3. However, the characteristic diffraction peaks of Fe_2O_3 are absent in the sample prepared in EG solvent, indicating that rGO–Fe_2O_3 could not be fabricated using EG as the solvent, probably because of the reducibility of EG. In addition, the characteristic (002) diffraction peak of graphite ($2\theta = 11°$) could be seen in the pattern of the GO sample. Nevertheless, the peak at 11° disappears in the patterns of samples of rGO and rGO–Fe_2O_3 composites, confirming the reduction of GO after solvothermal treatment.

3.2 Morphology and size characterization

The morphologies and sizes of GO, rGO, Fe_2O_3, and rGO–Fe_2O_3 samples (fabricated in different solvents) were characterized using SEM and TEM, and the results are shown in Fig. 3 and 4. SEM results (Fig. 3c) indicate that the Fe_2O_3 sample is composed of agglomerated spherical Fe_2O_3 nanoparticles with an average particle size of 130 nm. Evident

aggregation of the as-received graphite oxide (without ultrasonic treatment) could be seen in the SEM imagines. This is distinct from the TEM results which show that the oligomeric structure of graphene oxide is obtained after ultrasonic treatment of 30 min. GO can be considered as an oligomeric structure because ultrasonic treatment was performed in all preparation processes. Both SEM and TEM images (Fig. 3b) show the crimped structure of the as-prepared rGO, fabricated *via* the solvothermal method, which can be attributed to its extremely thin feature.

SEM results indicate that Fe_2O_3 nanoparticles were successfully anchored on the surface of graphene (Fig. 4(a)–(e)). However, the morphologies of the composites and the dispersion of the Fe_2O_3 nanoparticles were found to be significantly distinct for different solvents. When compared with the rGO–Fe_2O_3 composites fabricated in NBA, H_2O, NMP, EA and EG solvents, the composite obtained in DMF solvent presents a thinner structure (see Fig. 4). It is also significant that the distribution of Fe_2O_3 nanoparticles anchored on graphene is high even when using DMF as the reaction solvent, confirming that graphene could effectively prevent the aggregation of Fe_2O_3 nanoparticles. This phenomenon can be attributed to the better dispersion performance of DMF for both GO and rGO.[27,28] Nevertheless, the poor dispersion of rGO in H_2O, EA and EG solvents results in an inferior interaction between rGO and Fe_2O_3. Moreover, the composite obtained in the EG solvent shows a different morphology from other samples. This can be attributed to the distinct composition (confirmed by XRD results).

3.3 FT-IR analysis

In order to confirm the reduction of GO and the interaction between rGO and Fe_2O_3, FT-IR measurements were recorded to investigate the composition of GO, rGO, Fe_2O_3 and rGO–
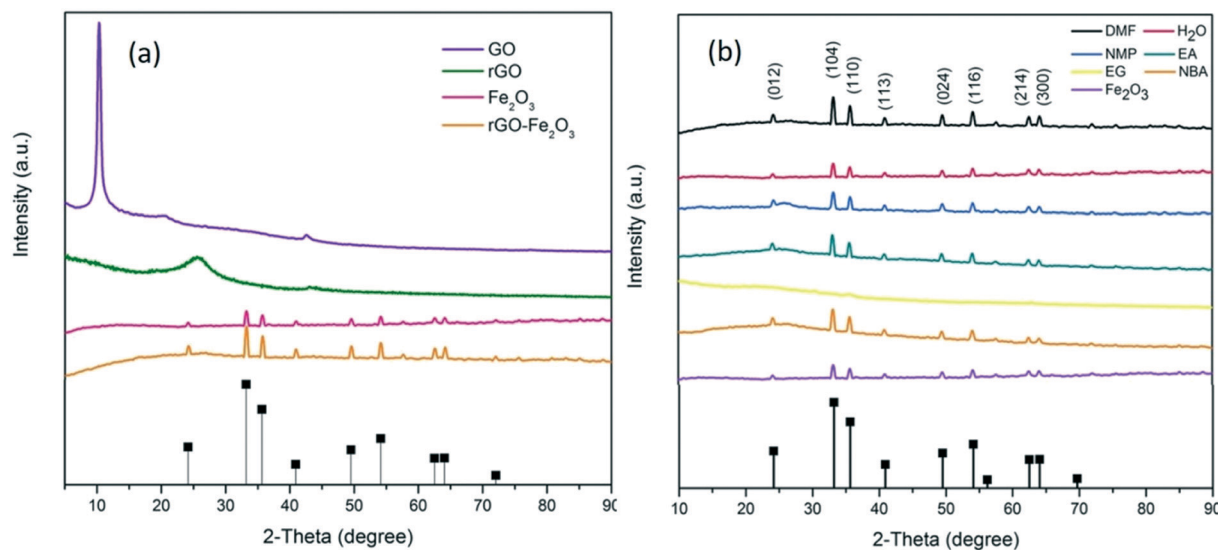

Fig. 2 XRD results of GO, rGO, Fe_2O_3 and rGO–Fe_2O_3 composites. (a) XRD results of GO, rGO, Fe_2O_3 and rGO–Fe_2O_3 (DMF) samples. (b) XRD results of rGO–Fe_2O_3 composites prepared in different solvents.
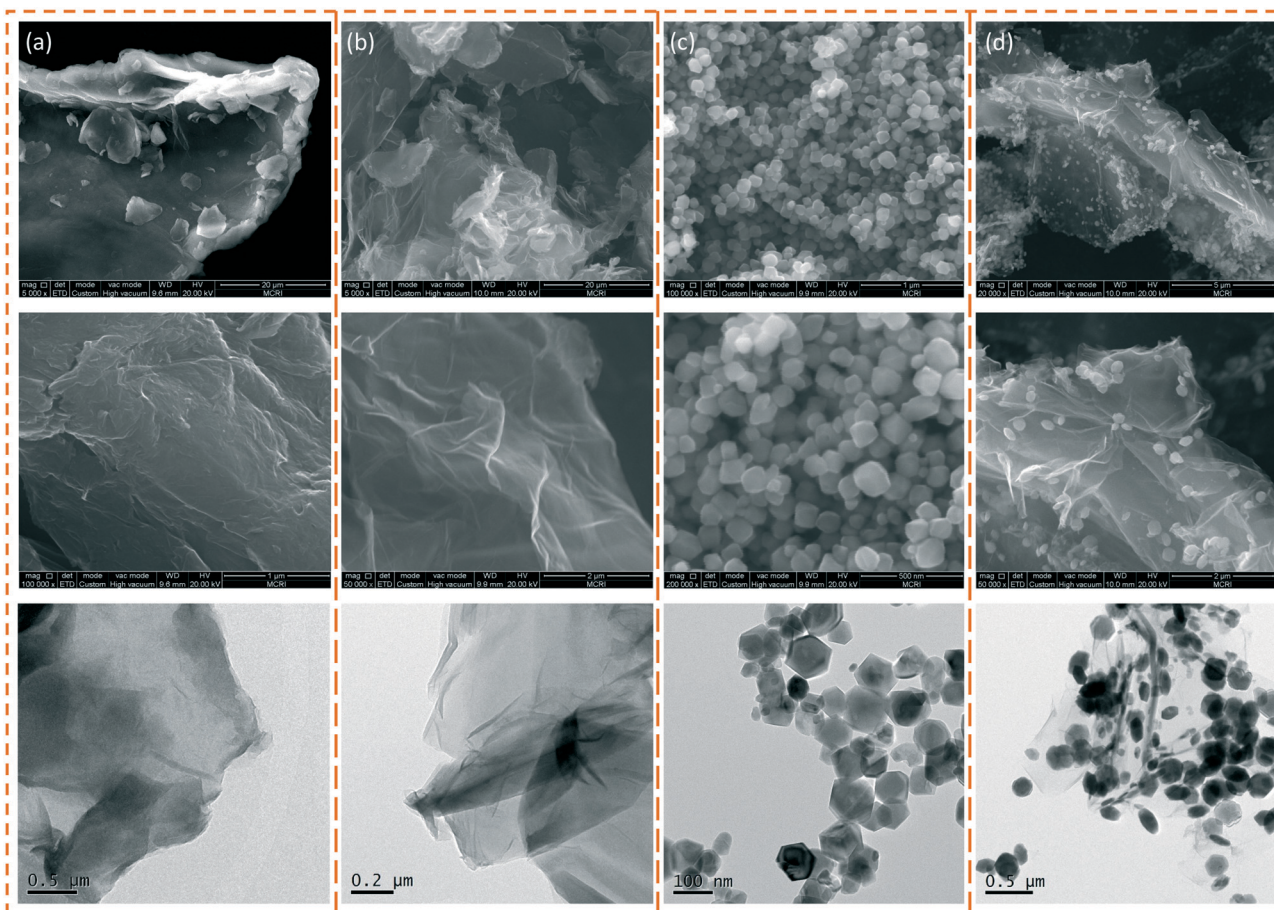
Fig. 3 SEM and TEM images of GO, rGO, Fe$_2$O$_3$ and rGO–Fe$_2$O$_3$ (DMF) samples: (a) GO, (b) rGO, (c) Fe$_2$O$_3$, and (d) rGO–Fe$_2$O$_3$ (DMF).
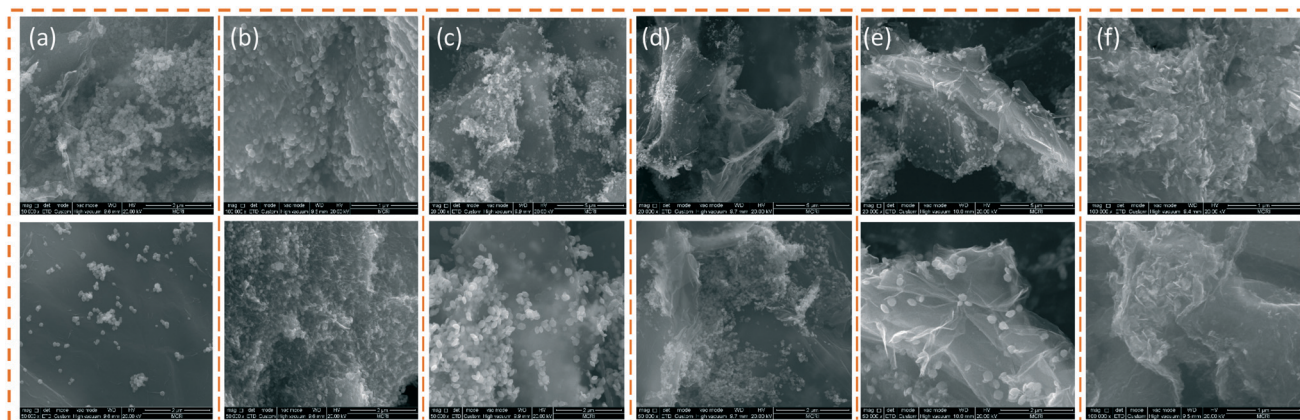

Fig. 4 SEM and TEM images of rGO–Fe$_2$O$_3$ composites fabricated in different solvents: (a) NBA, (b) H$_2$O, (c) EA, (d) NMP, (e) DMF, and (f) EG.

Fe$_2$O$_3$ composites. The corresponding spectra are shown in Fig. 5. Absorption peaks at around 3420 cm^{-1} (strong and broad) and 1625 cm^{-1} in GO sample are derived from the O–H stretching vibration and bending vibration of adsorbed water molecules, respectively. Moreover, the stretching vibration of C═O (COOH groups) situated at the surface and edge of GO sheets can be observed at 1730 cm^{-1}. For the pristine

Fe$_2$O$_3$, the strong peaks appear at 563 and 478 cm^{-1} (derive from the stretching vibration of Fe–O), which is consistent with previous studies that show the peaks of Fe–O appearing at around 470 cm^{-1} and 580 cm^{-1}.[29] The spectra of rGO and rGO–Fe$_2$O$_3$ composites differ from that of the GO sample, as evidenced by the significantly weaker peaks at 1625, 1730 and 3420 cm^{-1}, confirming the reduction of GO.
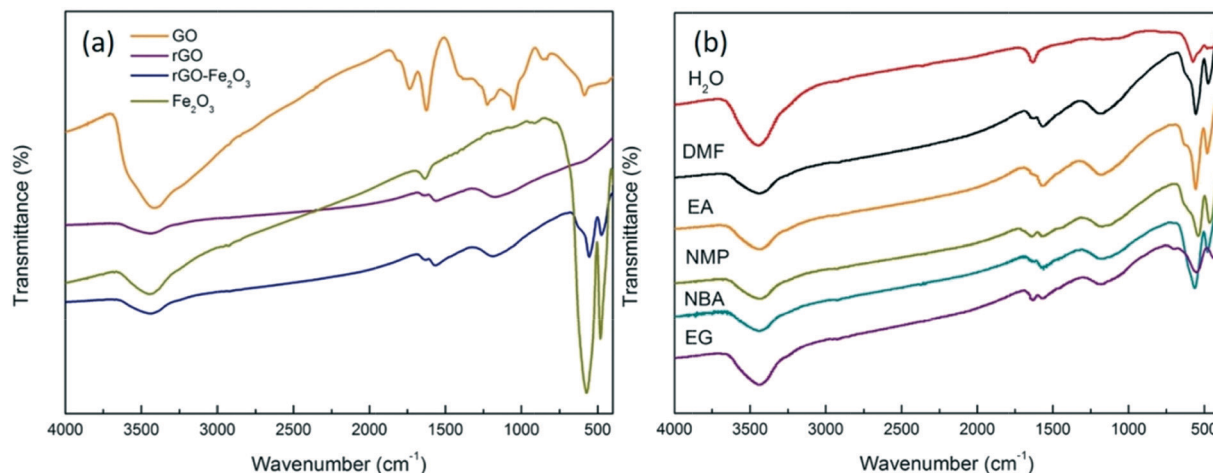
Fig. 5 FT-IR results of GO, rGO, Fe_2O_3 and rGO–Fe_2O_3 composites: (a) FT-IR results of GO, rGO, Fe_2O_3 and rGO–Fe_2O_3 (DMF) samples; (b) FT-IR results of rGO–Fe_2O_3 composites prepared in different solvents.

Moreover, the distinction of the Fe–O peak wavenumbers between the Fe_2O_3 (peaks at 563 and 478 cm^{-1}) and rGO–Fe_2O_3 (peaks at 555 and 474 cm^{-1}) samples also confirm the chemical interaction between the metal oxide and graphene.

Based on this finding, we could suspect that van der Waals' forces (physical adsorption, weak interaction) and chemical interactions (chemical bond, strong interaction) coexist between Fe_2O_3 nanoparticles and rGO.[24]
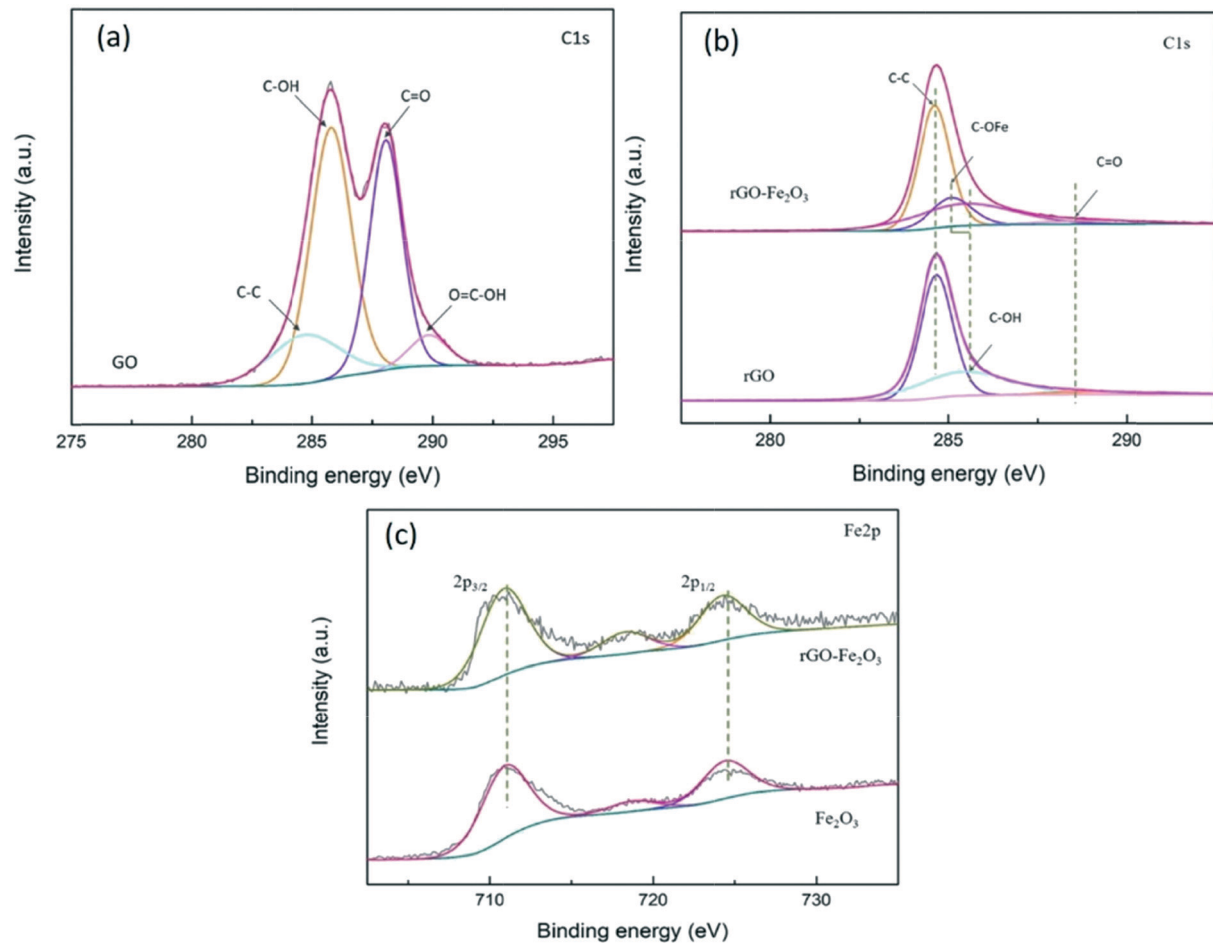

Fig. 6 XPS results of GO, rGO, Fe_2O_3 and rGO–Fe_2O_3 composites: (a) C 1s spectra of GO sample; (b) C 1s spectra of rGO and rGO–Fe_2O_3 (DMF) samples; (c) Fe 2p spectra of Fe_3O_4 and rGO–Fe_2O_3 (DMF) samples.

3.4 XPS analysis

XPS was performed to study the surface chemical composition and to identify the interaction between GO and Fe_2O_3. The results are shown in Fig. 6. The spectrum of C 1s (Fig. 6a) of GO can be divided into four main peaks at 284.6, 285.4, 288.5 and 288.8 eV, associated with C–C (sp^2-C), C–OH (oxygen in hydroxyl), C=O and HO–O=C (carboxyl) groups, respectively. However, only three peaks, associated with C–C (sp^2-C), C–OH (oxygen in hydroxyl) and C=O groups, appear in the C1s spectra of rGO sample. Moreover, the change in peak intensity (intensity reduction of C–OH and C=O groups, intensity increase of the C–C (sp^2–C) group) confirm the reduction of GO to rGO. Particularly, the C 1s peak of the rGO–Fe_2O_3 (DMF) sample located at 284.4 eV (refer to carbon in C–O–H bond) shifts toward 0.3 eV lower binding energy in comparison with that of rGO owing to the stronger interaction between O and Fe, indicating the formation of Fe–O–C bond.[31]

Additionally, it was found that peaks at around 711, 720 and 725 eV appearing in the spectra of Fe_2O_3 and rGO–Fe_2O_3 (DMF) samples are related to Fe 2p, providing clear evidence for the existence of Fe^{3+} on the surface of graphene (Fig. 6c). XPS results show the chemical interaction between GO and Fe_2O_3 and also indicate the reduction of GO to rGO after solvothermal treatment.

3.5 Raman analysis

The Raman spectra of GO, rGO, pristine Fe_2O_3 and rGO–Fe_2O_3 (DMF) samples are presented in Fig. 7. The Raman peak at around 1340 cm^{-1} (D band) is related to the defects and disorders in the hexagonal graphitic layers. In addition, the peak at 1580 cm^{-1} (G band), corresponding to an E_{2g} mode of graphite, is related to the vibration of sp^2-bonded carbon atoms in the 2-dimensional hexagonal lattice.[24] In the Raman spectrum of Fe_2O_3 sample, strong peaks at 214 cm^{-1}-

and 271 cm^{-1} are assigned to the A_{1g} mode and E_g mode, respectively. Typical peaks of hematite and graphene (D and G bands) appear in the Raman spectrum of the rGO–Fe_2O_3(DMF) composite, which reveals the formation of the rGO–Fe_2O_3 composite. The calculated I_D/I_G ratios of GO, rGO and rGO–Fe_2O_3 (DMF) samples are 2.75, 2.42 and 2.45, respectively. The distinction of the I_D/I_G ratios suggests an increase in sp^2 domains in the rGO and rGO–Fe_2O_3 (DMF) samples, confirming the reduction of GO to rGO, which is consistent with the XRD, FT-IR and XPS results. This also indicates the enhancement of the order degree after solvothermal treatment which concurs with previous studies.[23] Moreover, the enhanced I_D/I_G value of the rGO–Fe_2O_3 composite in comparison with that of rGO shows the decrease in the order degree, which is attributed to the interaction between Fe_2O_3 and rGO.

3.6 Thermal analysis

3.6.1 DSC results. The catalytic performance of GO, rGO, Fe_2O_3 and rGO–Fe_2O_3 composites on the thermal decomposition of AP was investigated by DSC. The results are shown in Fig. 8. The effects of different rGO–Fe_2O_3 samples (fabricated in different solvents) on the thermal decomposition of AP were also explored according to the DSC results. DSC results revealed that the thermal decomposition curve of pure AP contains one endothermic and two exothermic peaks. The endothermic peak appearing at 244 °C is attributed to the phase transition of AP from orthorhombic to cubic form. Exothermic peaks appear at 324 and 440 °C, corresponding to the LTP (low-temperature decomposition exothermic peak) and HTP of AP, indicating its full decomposition.

As can be seen from Fig. 8(a) and (b), in the DSC curve of AP, there is no distinct shift in the endothermic peak before and after the addition of GO, rGO, Fe_2O_3 and rGO–Fe_2O_3. However, the LTP and HTP of AP significantly change after
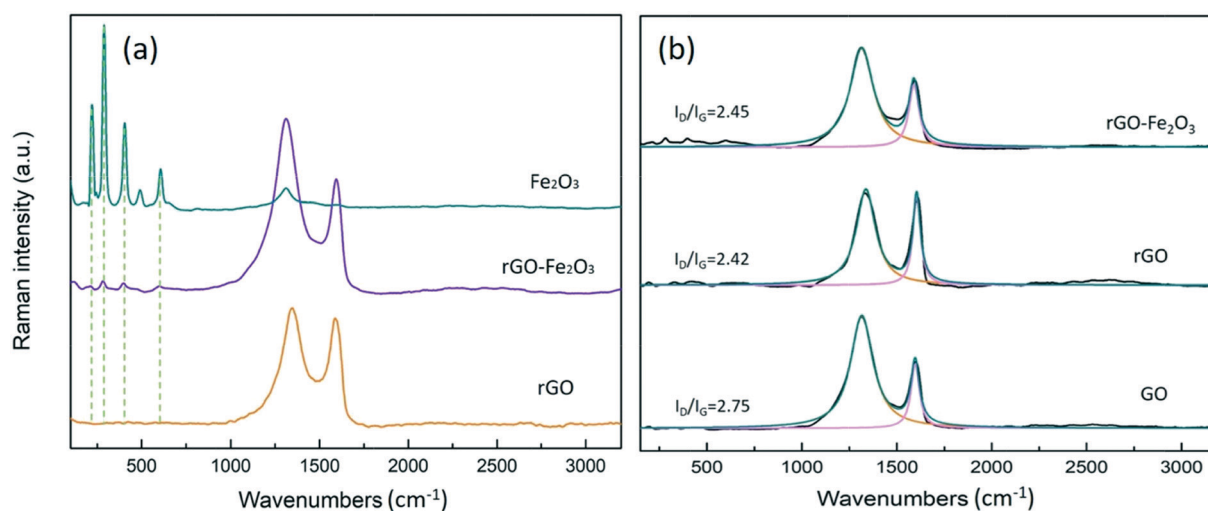

Fig. 7 RAMAN spectra of GO, rGO, Fe_2O_3 and rGO–Fe_2O_3 composites: (a) Raman peaks of rGO, Fe_2O_3 and rGO–Fe_2O_3 (DMF); (b) I_D/I_G values of GO, rGO and rGO–Fe_2O_3 (DMF).
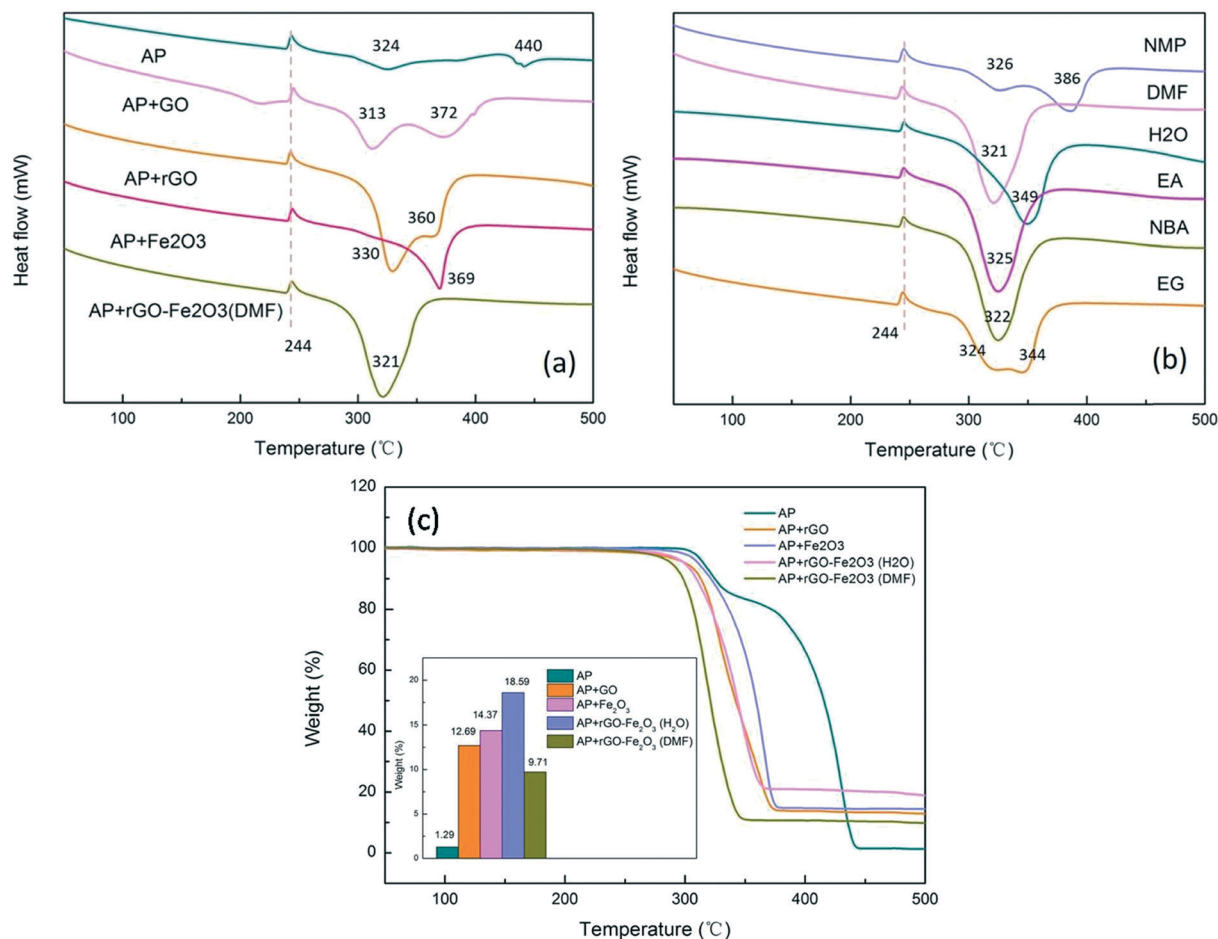
Fig. 8 DSC and TGA results of pure AP, AP mixed with rGO, Fe_2O_3 and rGO–Fe_2O_3 at 10 °C min^{-1}: (a) DSC results of pure AP and AP mixed with GO, rGO, Fe_2O_3 and rGO–Fe_2O_3 (DMF); (b) DSC results of AP mixed with different rGO–Fe_2O_3 samples; (c) TGA results of AP, AP mixed with rGO, Fe_2O_3, rGO–Fe_2O_3 (H_2O) and rGO–Fe_2O_3 (DMF).

mixing with GO, rGO, pristine Fe_2O_3 and rGO–Fe_2O_3 composites (see Table 1). The HTP of AP + GO and AP + rGO samples decrease by 68.3 and 79.2 °C, respectively, in comparison with the HTP of pure AP (440.8 °C). The better catalytic activity of GO and rGO on the thermal decomposition of AP resulted from the excellent thermal conductivity of the graphene materials, which was also confirmed by previous studies.[32,33]

Additionally, the rGO–Fe_2O_3 samples (fabricated in different solvents) present different effects on the thermal decomposition temperature of AP (Fig. 8b). The HTP of AP mixed with rGO–Fe_2O_3 composites fabricated in H_2O, DMF, EA, EG, NMP and NBA solvents reduced by 91.0, 119.6, 115.6, 96.1, 54.3 and 118.0 °C, respectively. The HTP of AP + rGO–Fe_2O_3 (fabricated in DMF solvent) advanced the maximum, demonstrating that the rGO–Fe_2O_3 (DMF) sample exhibits the best catalytic performance on the thermal decomposition of AP. It is clear that compared with the rGO–Fe_2O_3 (H_2O) sample, the rGO–Fe_2O_3 composite fabricated in DMF solvent presents higher catalytic activity on the thermal decomposition of AP, which indicates that DMF is more suitable as a solvent for rGO–Fe_2O_3 composite fabrication. Combining DSC and SEM results, we can conclude that the enhanced catalytic property of rGO–Fe_2O_3 (DMF) can be attributed to the uniform distribution of Fe_2O_3 nanoparticles anchored on graphene, which could provide more active sites for the decomposition of AP.

3.6.2 TG results. Fig. 8(c) illustrates the thermogravimetric results of AP (heated from 50 to 500 °C) mixed with GO, rGO, pristine Fe_2O_3, rGO–Fe_2O_3 (H_2O) and rGO–Fe_2O_3 (DMF). It can be seen that the pyrolysis behavior of AP contains two

Table 1 Thermal decomposition temperatures of AP mixed with different catalysts at 10 °C min^{-1}

Sample no.	Energetic material	Catalysts		LTP/°C	HTP/°C
		Name	Solvent		
1	AP	—	—	324.8	440.8
2		GO	—	313.5	372.5
3		rGO	H_2O	330.5	360.8
4		Fe_2O_3	H_2O	—	369.4
5		rGO–Fe_2O_3	DMF	—	321.2
6			NMP	326.5	386.5
7			H_2O	—	349.8
8			EA	—	325.2
9			NBA	—	322.8
10			EG	324.7	344.7

stages corresponding to the high temperature and low temperature decomposition exothermic processes (see DSC results). The residue quality of AP + rGO–Fe$_2$O$_3$ (DMF) sample is clearly lower than that of AP + rGO and AP + Fe$_2$O$_3$ samples, which also confirmed the excellent catalytic performance of rGO–Fe$_2$O$_3$ (DMF). Moreover, the high residual quality of the rGO–Fe$_2$O$_3$ (H$_2$O) sample shows its unsuitability for AP decomposition, which can be attributed to the poor dispersion of Fe$_2$O$_3$ nanoparticles.

3.6.3 Dynamics calculation. The apparent activation energy (Ea) of the thermal decomposition process of AP mixed with different additives was evaluated by Kissinger and Ozawa's methods using DSC data (see Table 2), and the results are listed in the Table 3. The apparent activation energies of the high temperature decomposition process for AP + GO, AP + rGO, AP + Fe$_2$O$_3$ and AP + rGO–Fe$_2$O$_3$ (DMF) are reduced by 76.9, 164.3, 122.8 and 173.3 kJ mol^{-1}, respectively, in comparison with 293.1 kJ mol^{-1} for pure AP. These results indicate that rGO–Fe$_2$O$_3$ (DMF) can effectively decrease the thermal decomposition temperature and apparent activation energy of AP, and presents an excellent catalytic effect on the thermal decomposition of AP.

3.7 Catalytic mechanism of the thermal decomposition of AP catalyzed by rGO–Fe$_2$O$_3$ composites

AP decomposition occurred *via* three steps: phase transformation, low temperature decomposition (LTD) and high temperature decomposition (HTD). In the first step, the phase of AP transforms from the orthorhombic phase to the cubic phase. LTD is a solid–gas multiphase reaction procedure, including decomposition and sublimation processes. HTD involves reactions between HNO and NO for the generation of N$_2$O, and the major products of HTD are N$_2$O, O$_2$, Cl$_2$, H$_2$O and some NO (shown in Fig. 1).[24] The electron transfer process from ClO$_4^-$ to NH$_4^+$ and from O$_2$ to the superoxide ion (O$_2^-$) are the controlling steps of LTD and HTD, respectively.[23] Then, the generated O$_2^-$ contributes to the decomposition of NH$_3$ in combination with the other products of HClO$_4$; eventually, the AP is completely decomposed.[24]

The possible mechanism by which the introduction of GO, rGO, Fe$_2$O$_3$ and rGO–Fe$_2$O$_3$ composites promote the thermal

Table 3 Kinetic parameters of AP obtained by Kissinger method and Ozawa's method

Sample no.	T_p/°C	Kissinger method			Ozawa's method	
		E_k/kJ mol^{-1}	L_g (A_k/s^{-1})	r_k	E_o/kJ mol^{-1}	r_k
1	LTP	124.2	8.73	0.986	127.5	0.988
	HTP	293.1	19.47	0.995	290.0	0.995
2	LTP	91.0	5.76	0.985	95.9	0.988
	HTP	216.2	15.55	0.981	215.8	0.983
3	LTP	116.7	7.89	0.996	120.5	0.997
	HTP	128.8	8.38	0.987	132.5	0.989
4	LTP	—	—	—	—	—
	HTP	170.3	11.73	0.996	172.1	0.997
5	LTP	—	—	—	—	—
	HTP	119.8	8.31	0.982	123.4	0.984

decomposition of AP are shown in Fig. 1. The excellent thermal conductivity and unique electronic structure of graphene materials (GO and rGO) benefit the heat transfer process and the rate controlling step of thermal decomposition of AP.[32,33] Therefore, the addition of graphene materials (GO and rGO) significantly reduced the HTP of AP. According to the traditional electron-transfer theory, the partially filled 3d orbit of Fe^{3+} benefits the transfer of electrons. When AP is mixed with Fe$_2$O$_3$, the positive holes of Fe$_2$O$_3$ can accept electrons from AP, thus promoting the thermal decomposition of AP.[24] Additionally, graphene can effectively inhibit the agglomeration of Fe$_2$O$_3$ nanoparticles, providing more active sites for the thermal decomposition of AP. Moreover, its excellent conductivity contributes to the transport of electrons. Based on the above discussion, the introduction of graphene could not only significantly reduce the agglomeration of Fe$_2$O$_3$, but also accelerate the transport of electrons to speed up the controlling steps of LTD and HTD. Hence, rGO–Fe$_2$O$_3$ (DMF) displays higher catalytic activity than pristine Fe$_2$O$_3$.[24] In addition, the enhanced dispersibility of Fe$_2$O$_3$ nanoparticles anchored on graphene is the primary reason for rGO–Fe$_2$O$_3$ (DMF) presenting better catalytic activity compared with that of other rGO–Fe$_2$O$_3$ samples.

4. Conclusions

The effect of different solvents on the structure and properties of rGO–Fe$_2$O$_3$ composites and the effect of the as-synthesized rGO–Fe$_2$O$_3$ composites on the thermal decomposition performance of AP were studied. rGO–Fe$_2$O$_3$ composites were successfully fabricated using different solvents *via* a solvothermal method, except when using EG as the solvent. The chemical interaction between rGO and Fe$_2$O$_3$ was confirmed by FTIR, XPS and Raman results. SEM results indicate that the distribution of Fe$_2$O$_3$ nanoparticles on graphene is more uniform while using DMF as the reaction medium, confirming that graphene effectively prevents the aggregation of Fe$_2$O$_3$ nanoparticles. In addition, DSC results also indicate that it is better to use DMF as the solvent for rGO–Fe$_2$O$_3$ preparation, which could effectively promote the thermal decomposition of AP with a significantly reduced

Table 2 Thermal decomposition temperatures of AP mixed with different catalysts at different heating rates

Sample no.	Energetic component	Catalysts	T/°C	β/°C min^{-1}			
				5	10	15	20
1	AP	—	LTP	307.9	324.8	329.0	339.3
			HTP	432.9	440.8	447.0	452.3
2		GO	LTP	300.2	313.5	329.0	339.3
			HTP	360.2	372.5	378.7	379.6
3		rGO	LTP	315.1	330.5	342.7	347.1
			HTP	346.8	361.6	375.6	377.7
4		Fe$_2$O$_3$	LTP	—	—	—	—
			HTP	358.1	369.4	379.3	383.8
5		rGO–Fe$_2$O$_3$ (DMF)	LTP	—	—	—	—
			HTP	310.2	321.2	332.2	341.0

decomposition temperature and apparent activation energy. Combining the results of SEM and DSC, we can infer that the higher catalytic activity of rGO–Fe$_2$O$_3$ (DMF) compared with that of other additives can be attributed to the excellent electroconductivity of graphene and better dispersibility of Fe$_2$O$_3$ nanoparticles, which could provide more catalytic sites for the thermal decomposition of AP.

Conflicts of interest

There are no conflicts to declare.

Acknowledgements

References

1 L. Meng, Z. Lu and X. Wei, et al., Two-sided effects of strong hydrogen bonding on the stability of dihydroxylammonium 5,5′-bistetrazole-1,1′-diolate (TKX-50), CrystEngComm, 2016, 18(13), 2258–2267.

2 R. Dubey, M. Chawla and P. F. Siril, et al., Bi-metallic nanocomposites of Mn with very high catalytic activity for burning rate enhancement of composite solid propellants, Thermochim. Acta, 2013, 572(43), 30–38.

3 P. Kumar, P. C. Joshi and R. Kumar, et al., Catalytic effects of Cu-Co* on the thermal decomposition of AN and AN/KDN based Green oxidizer and propellant samples, Def. Technol., 2018, 14, 250–260.

4 N. Li, M. Cao and Q. Wu, et al., A facile one-step method to produce Ni/graphene nanocomposites and their application to the thermal decomposition of ammonium perchlorate, CrystEngComm, 2011, 14(2), 428–434.

5 H. Kumar, P. N. Tengli and V. K. Mishra, et al., Synthesis and catalytic activity of Cu-Cr-O-TiO2 composites for the thermal decomposition of ammonium per-chlorate: enhanced decomposition rate of fuel for solid rocket motors, RSC Adv., 2017, 7(21), 12486–12495.

6 S. Elbasuney, A. Fahd and H. E. Mostafa, Combustion characteristics of extruded double base propellant based on ammonium perchlorate/aluminum binary mixture, Fuel, 2017, 208, 296–304.

7 L. N. Jin, Q. Liu and W. Y. Sun, Shape-controlled synthesis of Co3O4 nanostructures derived from coordination polymer precursors and their application to the thermal decomposition of ammonium perchlorate, CrystEngComm, 2012, 14(22), 7721–7726.

8 S. Isert, L. J. Groven and R. P. Lucht, et al., The effect of encapsulated nanosized catalysts on the combustion of composite solid propellants, Combust. Flame, 2014, 162(5), 1821–1828.

9 S. Tian, N. Li and D. Zeng, et al., Hierarchical ZnO hollow microspheres with exposed (001) facets as promising catalysts for the thermal decomposition of ammonium perchlorate, CrystEngComm, 2015, 17(45), 8689–8696.

10 S. Li, Z. Jiang and F. Zhao, et al., The effect of nano metal powders on the thermal decomposition kinetics of ammonium perchlorate, Chin. J. Chem. Phys., 2004, 17(5), 623–628.

11 Y. Chen, K. Ma and J. Wang, et al., Catalytic activities of two different morphological nano-MnO2, on the thermal decomposition of ammonium perchlorate, Mater. Res. Bull., 2018, 101, 56–60.

12 A. Dey, V. Nangare and P. V. More, et al., A graphene titanium dioxide nanocomposite (GTNC): one pot green synthesis and its application in a solid rocket propellant, RSC Adv., 2015, 5(78), 63777–63785.

13 N. Li, Z. Geng and M. Cao, et al., Well-dispersed ultrafine Mn 3 O 4, nanoparticles on graphene as a promising catalyst for the thermal decomposition of ammonium perchlorate, Carbon, 2013, 54(2), 124–132.

14 Y. Zhao, X. Zhang and X. Xu, et al., Synthesis of NiO nanostructures and their catalytic activity on the thermal decomposition of ammonium perchlorate, CrystEngComm, 2016, 18(25), 4836–4843.

15 G. Tang, Y. Wen and A. Pang, et al., The atomic origin of high catalytic activity of ZnOnanotetrapods for decomposition of ammonium perchlorate, CrystEngComm, 2013, 16(4), 570–574.

16 J. Wu, H. Zhang and T. Yao, et al., An Explosive Bomb-Inspired Method to Prepare Collapsed and Ruptured Fe2O3/Nitrogen-Doped Carbon Capsules as Catalyst Support, Chemistry, 2017, 23(67), 17095–17102.

17 Y. Lan, X. Li and G. Li, et al., Sol–gel method to prepare graphene/Fe2O3, aerogel and its catalytic application for the thermal decomposition of ammonium perchlorate, J. Nanopart. Res., 2015, 17(10), 395.

18 Z. Ma, F. Li and H. Bai, Effect of Fe2O3 in Fe2O3/AP Composite Particles on Thermal Decomposition of AP and on Burning Rate of the Composite Propellant, Propellants, Explos., Pyrotech., 2006, 31(6), 447–451.

19 M. A. Fertassi, K. T. Alali and Q. Liu, et al., Catalytic effect of CuO nanoplates, a graphene (G)/CuO nanocomposite and an Al/G/CuO composite on the thermal decomposition of ammonium perchlorate, RSC Adv., 2016, 6, 74155–74161.

20 Y. Zhang, L. Xiao and K. Xu, et al., Graphene oxide-enveloped Bi$_2$WO$_6$ composites as a highly efficient catalyst for the thermal decomposition of cyclotrimethylenetrinitramine, RSC Adv., 2016, 6(48), 42428–42434.

21 Y. Zu, Y. Zhao and K. Xu, et al., Preparation and comparison of catalytic performance for nano MgFe$_2$O$_4$, GO-loaded MgFe$_2$O$_4$, and GO-coated MgFe$_2$O$_4$, nanocomposites, Ceram. Int., 2016, 42, 18844–18850.

22 R. Shi, J. Zhao and S. Liu, et al., Nitrogen-doped graphene supported copper catalysts for methanol oxidative carbonylation: Enhancement of catalytic activity and stability by nitrogen species, Carbon, 2018, 130, 185–196.

23 A. Dey, J. Athar and P. Varma, et al., Graphene-iron oxide nanocomposite (GINC): an efficient catalyst for ammonium

perchlorate (AP) decomposition and burn rate enhancer for AP based composite propellant, *RSC Adv.*, 2014, **5**(3), 723–724.

24 Y. Yuan, J. Wei and Y. Wang, *et al.*, Hydrothermal preparation of Fe2O3 /graphene nanocomposite and its enhanced catalytic activity on the thermal decomposition of ammonium perchlorate, *Appl. Surf. Sci.*, 2014, **303**(6), 354–359.

25 R. Mendil, Z. B. Ayadi and K. Djessas, Effect of solvent medium on the structural, morphological and optical properties of ZnS nanoparticles synthesized by solvothermal route, *J. Alloys Compd.*, 2016, **678**, 87–92.

26 G. Zhu, P. Liu and J. Zhou, *et al.*, Effect of mixed solvent on the morphologies of nanostructured Bi2S3, prepared by solvothermal synthesis, *Mater. Lett.*, 2008, **62**(15), 2335–2338.

27 J. I. Paredes, S. Villarrodil and A. Martínezalonso, *et al.*, Graphene oxide dispersions in organic solvents, *Langmuir*, 2008, **24**(19), 10560.

28 S. Villar-Rodil, J. I. Paredes and A. Martínez-Alonso, *et al.*, Preparation of graphene dispersions and graphene-polymer composites in organic media, *J. Mater. Chem.*, 2009, **19**(22), 3591–3593.

29 Y. Wang, M. Zhang and D. Pan, *et al.*, Nitrogen/sulfur co-doped graphene networks uniformly coupled N-Fe2O3, nanoparticles achieving enhanced supercapacitor performance, *Electrochim. Acta*, 2018, **130**, 85–195.

30 J. K. Zhang, F. Q. Zhao and S. Y. Xu, *et al.*, Preparation of Fe2O3@rGO Nanocomposites and Their Effect on the Thermal Decomposition of TKX-50, *Hanneng Cailiao*, 2017, **25**(7), 564–569.

31 N. H. N. Azman, M. S. Mamat and N. L. Hong, *et al.*, High-performance symmetrical supercapacitor based on poly(3,4)-ethylenedioxythiophene/graphene oxide/iron oxide ternary composite, *J. Mater. Sci.: Mater. Electron.*, 2018, **29**(8), 6916–6923.

32 N. K. Memon, A. W. Mcbain and S. F. Son, Graphene Oxide/ Ammonium Perchlorate Composite Material for Use in Solid Propellants, *J. Propul. Power*, 2016, **32**(3), 1–5.

33 X. Wang, J. Li and Y. Luo, *et al.*, A novel ammonium perchlorate/graphene aerogel nanostructured energetic composite: preparation and thermal decomposition, *Sci. Adv. Mater.*, 2014, **6**(3), 530–537.